Earth and Planetary Science Letters 532 (2020) 116030

Contents lists available at ScienceDirect

Earth and Planetary Science Letters

www.elsevier.com/locate/epsl

Precipitation of multiple light elements to power Earth's early dynamo

Tushar Mittal [a,*], Nicholas Knezek [a], Sarah M. Arveson [b], Chris P. McGuire [c], Curtis D. Williams [d], Timothy D. Jones [f], Jie Li [e]

[a] Earth and Planetary Science Department, University of California, Berkeley, Berkeley, CA, USA
[b] Department of Geology & Geophysics, Yale University, New Haven, CT, USA
[c] School of GeoSciences, University of Edinburgh, EH9 3FE, United Kingdom
[d] Earth and Planetary Science Department, University of California, Davis, Davis, CA, USA
[e] Department of Earth and Environmental Sciences, University of Michigan, Ann Arbor, MI, USA
[f] Department of Terrestrial Magnetism, Carnegie Institution of Washington, Washington, DC, USA

ARTICLE INFO

Article history:
Received 19 August 2019
Received in revised form 8 December 2019
Accepted 9 December 2019
Available online 27 December 2019
Editor: J. Brodholt

Keywords:
core-mantle evolution
paleomagnetic field
light-element precipitation
thermo-chemical evolution
core formation

ABSTRACT

Earth has had a global magnetic field for at least 3.5 billion years, but if the iron-alloy in the core has high conductivity, it is difficult to explain this duration with energy from cooling and inner-core growth alone. Precipitation of light elements (e.g., magnesium, silicon, and oxygen) from Earth's core is a potential alternative energy source to power the dynamo. We develop a new framework of coupled thermo-chemical evolution of the Earth to consider precipitation of multiple light components from the core and their interaction with the overlying mantle layer. The precipitated material accumulates in a layer at the base of the mantle which is then continuously eroded by mantle convection. We allow the precipitation of three species (MgO, FeO, and SiO_2), including their interactions not considered by most previous studies. We find that MgO, SiO_2, and FeO precipitation may each dominate entropy production depending on the choice of equilibrium constants and initial model states and that the three species together can explain the duration of Earth's magnetic field across a range of plausible scenarios. Over the Earth's history, we find that the core can lose ~1–2 wt% silicon and oxygen suggesting that light precipitation is potentially an important process for the core compositional evolution and core-mantle chemical exchange. Additionally, our results show that precipitation does not, in most cases, have a systematic influence on the timing of inner-core nucleation or magnitude of the resulting paleomagnetic signal with inner-core nucleation typically around 550 Mya. However, the onset of precipitation of individual species could produce additional sharp increases in paleomagnetic intensity at various points through Earth's history besides the inner-core nucleation event.

1. Introduction

The Earth's magnetic field is generated by convection in the outer fluid core primarily driven at present-day by the compositional buoyancy provided by the expulsion of light elements from inner core growth. However, this mechanism may not have been operational throughout Earth's history. Recent experimental and theoretical calculations show that the thermal conductivity of iron at core temperatures and pressures may be much higher than previously assumed (Pozzo et al., 2012, 2013; de Koker et al., 2012; Gomi et al., 2013; Ohta et al., 2016; Williams, 2018) (see Supplementary Section S5; also Konopkova et al. (2016); Yong et al. (2019) suggest lower conductivity values). The thermal evolution models for the Earth motivated with these updated values consistently find that inner core solidification began only 1.5-0.5 Bya (Labrosse, 2015; Nimmo, 2015; Davies, 2015; Driscoll and Bercovici, 2014), which is broadly consistent with paleomagnetic measurements (Biggin et al., 2015; Bono et al., 2019) within large uncertainties. We have direct paleomagnetic evidence for a global magnetic field from at least 3.5 Bya onwards (Tarduno et al., 2015; Biggin et al., 2015), so the dynamo must have been powered by other mechanisms for the majority of the Earth's history. Thermal cooling provides energy for convection. However, models require either potentially too high initial core temperatures (concerning geochemical constraints on mantle cooling over the Earth's history, Keller and Schoene (2018) and references therein) or radioactivity (e.g. Du et al., 2017; Chidester et al., 2017) to power a dynamo for the required duration. Thus, there is potentially a "core paradox" to explain Earth's long-lived magnetic field (Olson, 2013).

* Corresponding author.
E-mail address: tmittal2@berkeley.edu (T. Mittal).

https://doi.org/10.1016/j.epsl.2019.116030
0012-821X/

The present-day outer core has a density deficit of 5-8% as well as anomalous seismic velocities with respect to the expectation for a pure Fe-Ni liquid (Poirier, 1994; Hirose et al., 2013). Consequently, the core must contain some additional light elements such as Si, S, O, C, N, and H. In addition, results from experiments as well as models of Earth' core formation (Fischer et al., 2017; Rubie et al., 2015; Badro et al., 2015, 2016), suggest that the initial core may have been heated to high enough temperatures to dissolve many wt % of abundant lithophile elements such as Mg, Si, and O (besides other light elements such as C, S, and H, as well as trace elements). Motivated by these results, several studies have proposed that as the Earth cools, light elements such as Mg (Badro et al., 2016; O'Rourke and Stevenson, 2016; Du et al., 2017; Badro et al., 2018), Si, and O (Hirose et al., 2017) become supersaturated in the core and precipitate into the lower mantle, leaving behind a denser core fluid. Analogous to the crystallization of the present-day inner core, this mechanism provides a compositional buoyancy source for entropy to drive the Earth's dynamo and magnetic field and leads to a corresponding change in the bulk core composition over Earth's history.

Most previous studies (e.g., Badro et al. (2016)) have focused on only a single light-element entropy source, but all three species: MgO, SiO_2, and FeO can precipitate simultaneously. Additionally, these three precipitation reactions are inherently coupled through the oxygen concentration in the core fluid, as also pointed out by Du et al. (2017). Thus, a self-consistent chemical evolution model of the core requires the addition of the FeO equilibrium reaction along with MgO and SiO_2.

Another critical feature of these equilibrium reactions is the strong influence of mantle composition on the light element precipitation from the core. The precipitation products themselves change the composition of the thin mantle layer in equilibrium with the core, leading to dynamic feedback that is coupled to mantle convection. This influence has not been considered in previous studies, which have typically assumed equilibrium of individual light elements with either pure phases (Hirose et al., 2017) or a fixed silicate composition (Badro et al., 2016). In this study, we develop a new framework to model the coupled thermo-chemical evolution of the Earth by combining models for Earth's thermal evolution and Earth's core energetics with a chemical model for the coupled light element precipitation from the core and its interaction with the overlying mantle layer.

The primary motivation of this study is to address two related questions. First, we examine the entropy available to drive the dynamo through Earth's history when including self-consistent feedback from the mantle (Nimmo, 2015). We are especially focused on ascertaining whether multiple light elements can provide the required entropy even if a single species is insufficient (e.g. Du et al., 2017).

Second, we calculate the compositional evolution of Earth's core from core formation to present-day. Recent estimates of initial core composition from planetary accretion models prefer a reduced core with more silicon than oxygen to reproduce the mantle composition, especially the composition of slightly siderophile elements (vanadium and chromium), moderately siderophile elements (nickel and cobalt) as well as Fe (Siebert et al., 2012; Rubie et al., 2015; Fischer et al., 2017; Piet et al., 2017) (Supplementary Figure S1 with constraints from Fischer et al. (2017); Siebert et al. (2013)). Similarly, we have constraints on the present-day composition from seismic observations and mineral physics studies (e.g. Badro et al. (2015); Oka et al. (2019)) (Supplementary Figure S1 with constraints from Badro et al. (2015); Alfè et al. (2004)). Using our model, we assess the role of light element precipitation in the evolution of the core's light element composition, and we test if there are potential thermo-compositional histories that can connect estimates of initial and current core compositions. Finally, we also analyze the core's available entropy through time for any potentially observable features in paleomagnetic records.

2. Model description

We model Earth's thermal evolution using a coupled core-mantle thermodynamic model following the methods of Stevenson et al. (1983) for parameterized mantle convection and Nimmo (2015) for core thermodynamics. To this system of equations, we add equilibrium chemical reactions between the core and the mantle. Material that precipitates out of the core builds up in a thin mantle layer, altering its composition over time. This thin layer also moves with the background mantle convection, which brings fresh material in contact with the core and removes precipitated elements over time and setting up the "conveyor belt" system depicted in Fig. 1. The evolving layer composition governs the precipitation of light elements from the core into the mantle, which contributes to the heat and entropy budget of the Earth. These coupled relations are cast as a system of first-order Ordinary Differential Equations (ODEs) and solved forward in time from Earth's formation (post Moon-forming impact) to the present day.

Because we wish to model the precipitation of Mg and Si out of the core, we only track (Mg, Fe)SiO_3 in the mantle and do not include Ca-containing or Al-containing bridgmanite. Similarly, we track (Mg, Fe)O ferropericlase and SiO_2 but do not consider calcium-silicate perovskite ($CaSiO_3$). We track Fe, Mg, Si, O in the core as individual species. These species exchange with the mantle through the following equilibrium reactions:

$$MgO^{(mantle)} \leftrightarrow Mg^{(metal)} + O^{(metal)} \tag{1}$$

$$SiO_2^{(mantle)} \leftrightarrow Si^{(metal)} + 2O^{(metal)} \tag{2}$$

$$FeO^{(mantle)} \leftrightarrow Fe^{(metal)} + O^{(metal)} \tag{3}$$

as is schematically illustrated in Fig. 1.

The composition of the mantle interaction layer consists of MgO, SiO_2, FeO, $MgSiO_3$, and $FeSiO_3$. The total number of moles of each species are tracked and governed by the following equilibrium reactions:

$$MgSiO_3 \leftrightarrow MgO + SiO_2 \tag{4}$$

$$FeSiO_3 \leftrightarrow FeO + SiO_2 \tag{5}$$

$$FeSiO_3 + MgO \leftrightarrow FeO + MgSiO_3 \tag{6}$$

A detailed discussion of our model framework and assumptions is provided in Supplementary Section S2, S3 and S4. In the following, we highlight a couple of the key features of our model and parameter choices.

2.1. Interaction layer dynamics

In order to model the "conveyor belt" system, we include a layer erosion term in our ODE system to bring the layer composition back to the background mantle composition. We initialize the interaction layer to be in equilibrium with the initial core fluid. Along with the chosen layer thickness, this condition sets the initial total number of moles M_i of each species i in the layer. The time evolution of the layer composition is controlled by the rate of light element precipitation as well as advective mixing rate with the background mantle ($M_{i,b}$, a background mantle layer of equivalent thickness to the interaction layer). In order to model this later processes, we created an empirical function that pushes the mantle interaction layer composition towards the background mantle composition over a e-folding timescale τ

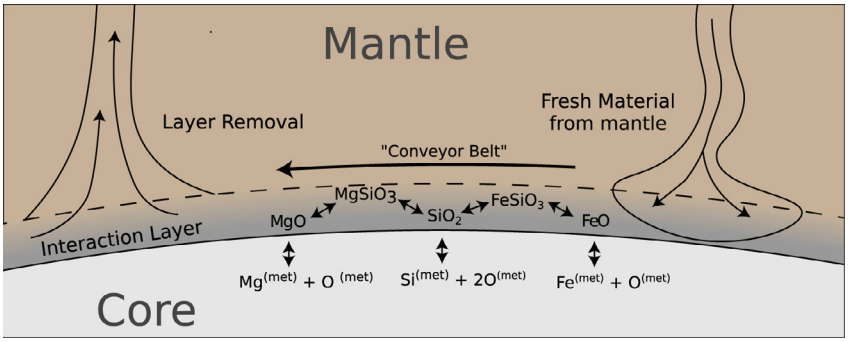

Fig. 1. Schematic representation of the chemical and dynamic interactions between Earth's core and mantle.

$$\left(\frac{dM_i}{dt}\right)_{erosion} = \frac{sgn(M_{i,b} - M_i)}{\tau}[(|M_i/M_{i,b} - 1| + 1)^2 - 1] \quad (7)$$

This equation can be easily converted into a derivative with respect to temperature for compatibility with the thermodynamic model using the change in CMB $\frac{dT_c}{dt}$ to obtain

$$\left(\frac{M_i}{dT}\right)_{erosion} = \frac{\left(\frac{M_i}{dt}\right)_{erosion}}{\frac{dT_c}{dt}} \quad (8)$$

In the absence of continued precipitation, this expression returns the layer composition to the background mantle composition on the timescale of mantle convection $\sim 10\tau$. In present day, the total timescale for material advection along the outer core boundary is order 600 Mya using an average mantle velocity equal to a typical surface plate speed of 6 cm/yr (Müller et al., 2016). Consequently, in this study, we assume a present day τ_p of 60 Mya. Since the mantle interior velocities scale directly with the mantle Rayleigh number (Foley and Bercovici, 2014), we expect τ to be smaller for early Earth which has had more vigorous convection. Consequently, we set $\tau_0 = \tau_p/8$ based on the median value of high surface velocities estimated using paleomagnetic data for early Earth (Piper, 2013; Weller and Lenardic, 2018). At intermediate times t, we set the τ using an exponential relationship varying between these values with a exponential timescale T_{tau} of 1 Bya:

$$\tau(t) = \tau_0 + (\tau_p - \tau_0)(1 - e^{\frac{-t}{T_{tau}}}) \quad (9)$$

2.2. Equilibrium coefficients

We compute equilibrium constants for each core and mantle species (MgO, FeO, and SiO_2) using the form used to fit a variety of experimental datasets:

$$K_i = 10^{a+b/T+cP/T} \quad (10)$$

There is considerable debate about the value of equilibrium constants at CMB temperatures and pressures, leading previous studies to conclude that either Mg or Si precipitation is the dominant source of entropy to power the dynamo. We model the evolution of the Earth using two sets of published equilibrium constants to compare results, which we call Parameter Set 1 and Parameter Set 2 (Table 1). For both the Parameter Sets 1 and 2, we use the equilibrium values for the MgO reaction from Badro et al. (2016). In Parameter Set 1, we use Fischer et al. (2015) for the constants for the SiO_2 and FeO reaction while we use Hirose et al. (2017) for the corresponding equilibrium constants in Parameter Set 2.

We did not incorporate the full expression given in Hirose et al. (2017) since it introduces numerical complexities in our model due to non-zero activity coefficient terms (see discussion in Supplementary material S2.2 of our choice of setting all the activity values to unity). We however found that adding a factor of 2 empirical correction provides a fairly accurate approximation to the full expression given in Hirose et al. (2017) over the range of changing silicon and oxygen contents in our calculations. Consequently, for Parameter Set 2, the value for K_{SiO2} is:

$$K_{SiO_2} = 2\left(K_{SiO_2,P1}\right)\left(K_{FeO,P2}\right)^2 \quad (11)$$

where $K_{SiO_2,P1}$ and $K_{FeO,P2}$ are the equilibrium constants for SiO_2 and FeO from Parameter Sets 1 and 2, respectively. Finally, since the variation between the Parameter Set 1 and Parameter Set 2 values is larger than the reported uncertainty in the fit values for the equilibrium constants in each study, we chose to fix the parameter value to the reported best-fit value from each study.

Table 1
Equilibrium constants for two different parameter sets. We use the equilibrium values for the MgO reaction from Badro et al. (2016) for both parameter sets. In Parameter Set 1, we use Fischer et al. (2015) for the constants for the SiO_2 and FeO reaction. In Parameter Set 2, we use values from Hirose et al. (2017).

Equilibrium constant	Parameter Set 1	Parameter Set 2
a_{MgO}	1.23	1.23
b_{MgO} (K)	−18816	−18816
c_{MgO} (K/GPa)	0	0
a_{FeO}	0.60	−0.3009
b_{FeO} (K)	−3800	0
c_{FeO} (K/GPa)	22	−36.8332
a_{SiO2}	1.3	(see text)
b_{SiO2} (K)	−13500	(see text)
c_{SiO2} (K/GPa)	0	(see text)

2.3. Thermodynamic model

We modified the Nimmo (2015) model by including gravitational and latent energy release through precipitation in the computation of heat evolution with $\tilde{Q}_{g,ex} = \tilde{Q}_{g,MgO} + \tilde{Q}_{g,FeO} + \tilde{Q}_{g,SiO2}$ and similarly for $\tilde{Q}_{L,ex}$. Here, $\tilde{Q}_i = Q_i/\frac{T_c}{dt}$ simply denotes a change from time to temperature derivatives (see Eqn. 73 in Ref. Nimmo (2015)). The other terms contributing to the energy balance for the core include terms associated with inner core growth (latent heat $\tilde{Q}_L$ and gravitational energy release $\tilde{Q}_g$), secular cooling $\tilde{Q}_s$, and energy production from volumetric radioactive heating in the core (Q_R, See Supplement S). The overall energy conservation equation for the core is:

$$\tilde{Q}_T = \tilde{Q}_s + \tilde{Q}_g + \tilde{Q}_L + \tilde{Q}_{g,ex} + \tilde{Q}_{L,ex} \quad (12)$$

$$Q_{CMB} = Q_R + \tilde{Q}_T \frac{T_c}{dt} \quad (13)$$

where Q_{CMB} is the CMB heat flux. Correspondingly, the entropy available to drive a dynamo field is:

$$\Delta E = E_R + \tilde{E}_T \frac{dT_c}{dt} - E_k \tag{14}$$

where E_R is the entropy production from radioactive heating, E_k is the entropy change due to thermal diffusion in an adiabatic core and $\tilde{E}_T$ includes the corresponding terms to $\tilde{Q}_T$ except the latent heat from precipitation. This latent heat term does not contribute to the entropy production in the core as heat released at the CMB does not contribute to thermal convection. In our model, inner core growth does not change the composition of the outer core but does contribute to the core thermal and entropy evolution. Additionally, we only allow Mg, Si, and O to precipitate out of the core but do not allow the reverse direction. We assume that any light elements that dissolve from the mantle into the core fluid would form a thin stratified layer at the CMB which would remain buoyantly stable.

As described in the Supplementary section S2.5, we obtain time evolution equations for the chemical components in the core and the mantle layer. We start the model with some initial temperatures for CMB (T_{CMB}) and upper-mantle (T_{UM}) $T_{c,0}$ and the initial composition of the core $M_{Fe}, M_{Mg}, M_{Si}, M_O$. We set the initial interaction layer composition by requiring it to be in equilibrium with the core at the initial temperature. At each subsequent timestep in the model, we then use the model to calculate the evolution of T_{CMB}, T_{UM}, and molar concentrations M_i over time to calculate the light element precipitation (see Supplementary section S3).

3. Results & discussion: entropy evolution

With this model framework, we calculate the coupled thermochemical evolution of the Earth's core and mantle starting with initial conditions of a core temperature and a core fluid composition of X_{Mg}, X_{Si}, and X_O (X_i are mole fractions of i = Mg, Si, and O) with the other parameters as described in the previous section (also see Supplement Section S1).

We first illustrate the importance of coupled core-mantle chemical exchange and mantle interaction layer dynamics. Since the principal motivation of our study is to address the "core paradox" of Earth's long-lived magnetic field, the primary variable of interest is the entropy available for magnetic field generation (Supplementary Material S2.3). Although the amount of entropy required for the present-day field is very uncertain, most estimates are on the order of a few hundred MW/K (Nimmo, 2015). We discuss the evolutionary history of the core for a fixed set of initial conditions to describe typical model behavior. We follow this discussion by exploring different evolution histories wherein light element precipitation (either MgO, FeO, or SiO_2) or secular cooling terms dominates the entropy production.

3.1. Importance of coupling terms

Since our model framework is significantly more complicated than most previous studies (e.g. Hirose et al., 2017), it is crucial to examine whether this added complexity has an impact on the evolutionary histories. We examine this by performing model simulations with the various entropy contributions terms wherein we start with the same initial conditions and systematically switch off various components of our additional model. Fig. 2 shows the results of this analysis with the various entropy contributions term as well as the available entropy. All panels use the same initial conditions of a core temperature of 5700 K and a core fluid composition of X_{Mg}: 0.01, X_{Si}: 0.12, and X_O: 0.08 along with Parameter Set 1 for the equilibrium coefficients.

In the base case (Fig. 2*a*), precipitation of MgO, FeO, and SiO_2 all operate, and the interaction layer is removed on the timescale τ. In Fig. 2*b*, the only light element allowed to precipitate from the core is FeO. In Fig. 2*c* and Fig. 2*d* we prevent the precipitation of MgO and SiO_2 respectively. We also explore two endmember cases for the removal of the interaction layer wherein the layer is not removed (Fig. 2*e*, very large τ) or the layer is removed instantly (Fig. 2*f*, very small τ).

In comparison to the base case, the light element precipitation and available entropy histories for each of the test cases are substantially different. Preventing the precipitation of one of the three light elements can strongly affect the precipitation history of the other species through both the coupled reactions as well as an influence on the core's cooling rate (Fig. 2, cases *a*, *b*, *c*, and *d*). Furthermore, we find that depending on the model choices, different light elements may precipitate out even with the same starting conditions. For instance, FeO only precipitates from the core when Mg is not allowed to enter the mantle (cases *a* vs. *b* and *c*). As a consequence, it should not be surprising that different choices for the scope of analysis, for example, including only Mg or Si precipitation, give different results compared to the fully coupled base case.

We also find that the total entropy available for dynamo action in the core is substantially larger for the base case (case *a*) vis-a-vis cases where some of the elements are not allowed to precipitate out (cases *b*,*c*, and *d*). In Fig. 2*b* and Fig. 2*c*, there are some parts of Earth's history wherein the available entropy is potentially insufficient. However, this is not the case for the base case *a*. Finally, we find that the rate of layer removal has a substantive impact on both the composition and rate of the light element precipitate. When the thin mantle layer is not swept away by mantle convection (as has been assumed by most prior studies), precipitation of all three species occurs with a continuous precipitation history (case *e*). In contrast, instantaneous layer removal suppresses precipitation of some oxides and leads to the initiation of different species precipitating at different discrete periods in Earth's history (case *f*).

3.2. Thermal and entropy evolution history

We illustrate the model behavior using an example model result for an initial core temperature of 5700 K, Parameter Set 1 for the equilibrium coefficients, and the core fluid composition of X_{Mg}: 0.01, X_{Si}: 0.12, and X_O: 0.08 (see Methods Section for other model parameters). The entropy and Core-Mantle Boundary heat flow results of this calculation are shown in Fig. 3.

Initially, the core cools rapidly as illustrated by the high CMB heat flow. There is a consequent high entropy production from super-adiabatic cooling (blue dashed curve) and radioactive components (green dotted curve) in the core. As the core cools, the Si in the core fluids gets supersaturated and starts to precipitate out at about 4 Bya before present (dark green curve). The precipitation of Si provides an entropy source since the core fluid left behind has a higher fraction of Fe and is thus denser, providing a compositional buoyancy source. Since compositional buoyancy is an efficient source of entropy to drive core convection, SiO_2 precipitation leads to a net increase in the available entropy at around 4 Bya. Additionally, the precipitation of SiO_2 has an associated latent heat, which leads to a sharp reduction in the core cooling rate. With further heat loss, the Si precipitation continues until the core-mantle composition and temperature conditions reach Mg saturation in the core around 2.8 Bya before present. MgO precipitation has an analogous influence on entropy and heat flow as SiO_2 has. The consequent reduction in core cooling rate, as well as the change in mantle layer composition, reduces the rate of SiO_2 precipitation (see Fig. 3). Nevertheless, the attendant drop in en-

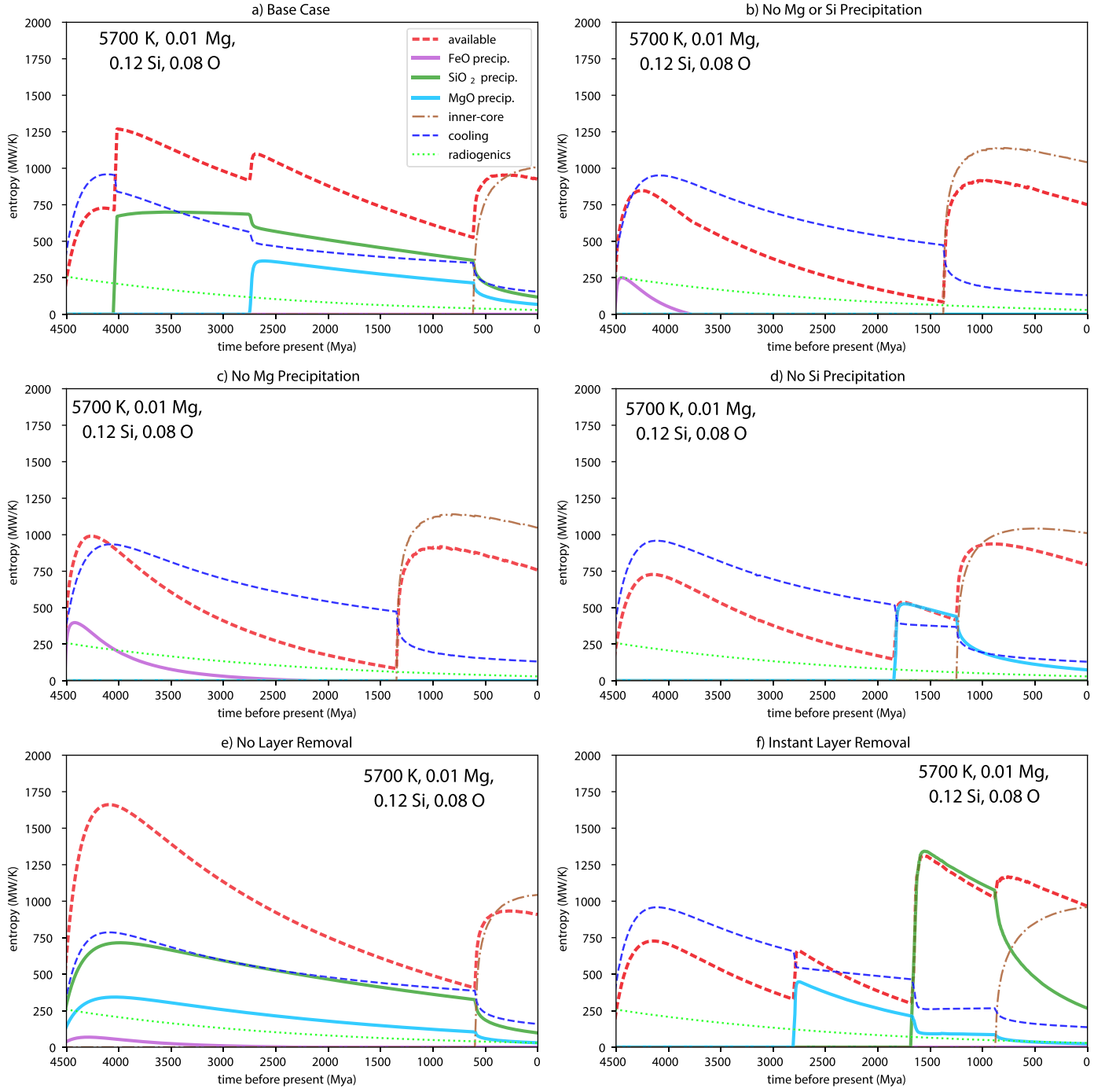

Fig. 2. Comparison of model results for fixed initial conditions and varying precipitate components and layer removal timescale. (a) The reference case wherein precipitation of MgO, FeO, and SiO_2 are all turned on, and the interaction layer is removed on a timescale τ. Other panels show the entropy history for cases with no MgO or SiO_2 precipitation (b), No MgO precipitation (c), No SiO_2 precipitation (d), the interaction layer is not removed (e), and the interaction layer is removed instantaneously (f).

tropy is counter-balanced by Mg related precipitation leading to a net increase in available entropy at MgO precipitation initiation. Finally, inner core nucleation around 600 Mya before present significantly reduces the core's cooling rate with the latent heat from ICB dominating the net CMB heat flow. This cooling rate reduction suppresses precipitation of both Mg and Si from the core, and inner-core entropy production dominates over all other sources. This model example clearly illustrates the role of different light element precipitates as sources of available entropy during Earth's history as well as their direct coupling with the core thermodynamics and mantle composition.

3.3. Representative histories with different dominant sources of entropy

We find that all three light element species: MgO, FeO, and SiO_2 can precipitate from the core during the Earth's history with the precipitation rate and dominant precipitation component varying substantially depending on the initial core composition and chosen equilibrium constants. As an illustration, we show representative model results in Fig. 3 where the largest time-averaged entropy source (main source) ranges from SiO_2 precipitation in Fig. 3a, MgO precipitation in Fig. 3b, cooling in Fig. 3c, and FeO in Fig. 3d. The results for Fig. 3a, b, and c use equilibrium values

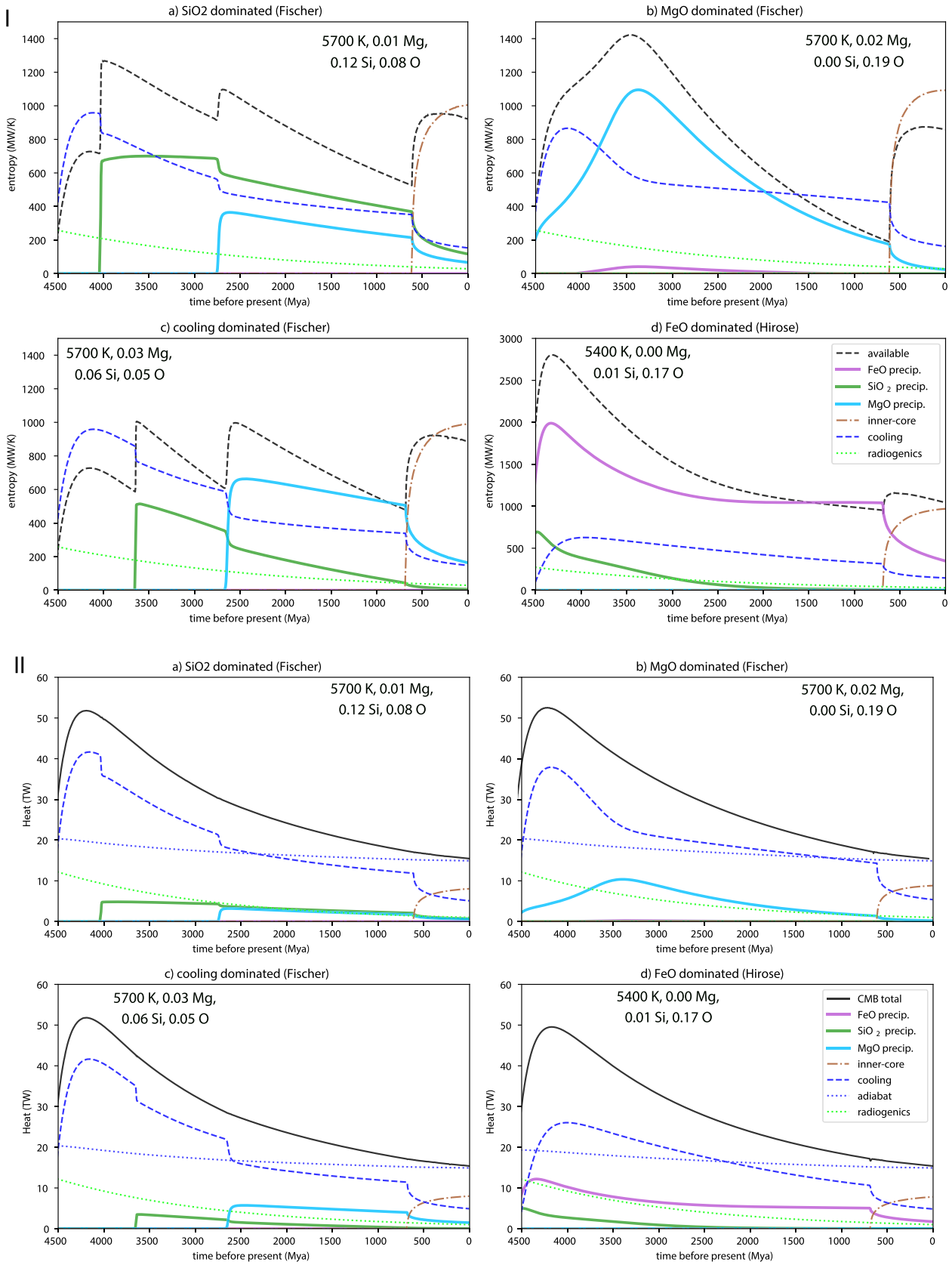

Fig. 3. Entropy production in the core (I) and Core Mantle Boundary heat flow (II) over Earth's history for four different representative parameter sets with varying initial concentrations of Mg, Si, and O that represent results in which SiO_2 precipitation dominates (Parameter Set 1) (a), MgO precipitation dominates (Parameter Set 1) (b), cooling dominates (Parameter Set 1) (c), and FeO precipitation dominates (Parameter Set 2) (d). The input parameter values for each model run are stated on the respective figure panel. (For interpretation of the colors in the figure(s), the reader is referred to the web version of this article.)

from Badro et al. (2016); Fischer et al. (2015) (Parameter Set 1) while Fig. 3d result uses Badro et al. (2016); Hirose et al. (2017) (Parameter Set 2) values. The initial core temperatures and initial amounts of Mg, Si, and O in the core vary between the four cases and are labeled in the figure.

It is important to note that even in cases for a single dominant entropy source, multiple other sources may still provide a significant contribution to the total available entropy. For instance, for the cooling dominated model run (Fig. 3c), a substantial amount of entropy is provided by light element precipitation. These model results highlight why a self-consistent coupling of the core-mantle chemical interaction is critical since it strongly affects the initiation time and rate of light element precipitation.

4. Results & discussion: parameter space exploration

The primary parameters in our model are the initial core temperature, the core fluid composition (X_{Mg}, X_{Si}, and X_O), and the two sets of choices for equilibrium constants - Parameter Set 1 and 2. Since initial conditions are not well constrained for the early Earth due to the uncertainties of temperatures, pressures, and core compositions in the core formation processes (e.g. Badro et al., 2016; Fischer et al., 2017), we sampled from a wide parameter space for each Parameter to explore the possible range of entropy histories and assess the ability of multiple light elements to provide the required entropy (see Supplementary Material S1 for the parameter ranges and other parameters).

4.1. Valid models

From amongst the wide parameter space results, we chose only results where

- Present-day inner core size is within 10% of the measured value of 1220 km
- Available entropy for driving the dynamo is greater than zero for the whole Earth history
- Either the present-day core composition matches seismic constraints (Badro et al., 2015) and minimum oxygen requirement for inner core density jump (Alfè et al., 2002) or the initial core fluid compositions is based on planetary accretion models (Siebert et al., 2012; Rubie et al., 2015; Fischer et al., 2017) (see Supplementary Fig. S1 for a permissible range of Si and Oxygen in the core fluid).

We follow the terminology in Fischer et al. (2017) to describe combinations of core Si, O concentrations as reference reduced case (preferred model case with results similar to their reduced case) wherein all accreted planetary material originating inside of 2 AU has an oxygen fugacity fO_2 of IW-3.5 while that from outside of 2 AU is oxidized (IW-1.5). Additionally, the oxidized case refers to the scenario wherein all the accreted material has an oxygen fugacity fO_2 of IW-1.5). The mean bulk planetary oxidation state at the end of accretion for these two cases is -2.3 (reference reduced) and -1.47 (oxidized) relative to the IW buffer (Fischer et al., 2017). The former is close to the current redox of the bulk Earth of around -2.3 (Siebert et al., 2013). The parameter space for the reference reduced and oxidized core Si and O composition is marked by the green and red boxes in Supplementary Figure S1. We also include another estimate of the Si and O content of the core from a similar type of analysis by Siebert et al. (2012) as a yellow envelope in Supplementary Figure S1.

Similarly, we use the constraints for present-day composition from Badro et al. (2015). The black line in Supplementary Figure S1 denotes a region including up to 3 wt% S and 7 wt% C, while the purple shaded region includes no C or S, i.e., the core composition required to satisfy seismic observations with only Si and O. Finally, it has been suggested that at least 2 wt% oxygen in the present day core is required to explain the observed inner-core boundary density jump 2 wt% oxygen (Alfè et al., 2002). We use this as an additional constraint in concert with the seismic based constraints from (Badro et al., 2015).

In our model, the present-day CMB temperature is not a free parameter, as we require the inner-core size to match the present-day inner core within 10%. As a consequence, the CMB temperature at present is automatically constrained to be within $\sim$10% of the 4180 K value from Nimmo (2015) since we use their formulation to compute the core adiabat to find the inner-core radius from CMB temperature. Since we do not include a change in core fluid composition due to inner core growth, our modern-day light element compositions will be biased slightly too low. However, since the inner core represents only 5% of the core's mass, we do not expect its crystallization and growth will not significantly change the bulk outer core light element concentration, especially given the other uncertainties in the compositional constraints (e.g., Nimmo (2015); Badro et al. (2015)).

4.2. Valid entropy histories

We show the available entropy over time for the subset of valid histories from our model in Fig. 4a (for Parameter Set 1) and Fig. 5a (for Parameter Set 2). The dominant source of entropy through Earth's history colors each line. If cooling produces the majority of entropy of Earth's history, the line is colored red; otherwise, the line is colored according to the light-element that provides the largest time-averaged entropy source over Earth's history: MgO (blue), FeO (pink), and SiO_2 (green). In other panels of Fig. 4 (b-d) and Fig. 5 (b-e), we show the fractional contribution of the cooling term, SiO_2, MgO, and FeO precipitation to the total available entropy over time.

We find that a wide variety of entropy histories are possible depending on the initial composition and temperature of the core. The entropy available for magnetic field generation throughout Earth's history ranges from $0.3\times$ to $4\times$ the present-day value but is almost always sufficient to drive a dynamo over the whole Earth's history. In all histories, we find that even if the entropy production is dominated by one term, the other sources typically still provide significant contribution (also see discussion in Section 3.3). This result again highlights the importance of coupling the precipitation of multiple light element species consistently.

For Parameter Set 1 (Fig. 4), the dominant entropy source in our valid models is either cooling or precipitation of SiO_2 or MgO with a minor contribution from FeO. Interestingly, we find that sudden increases in available entropy occur once or multiple times in many histories between 4.5 and 2.5 Bya as different species cross their equilibrium thresholds and begin to precipitate. Post 2.5 Bya, the entropy histories are smooth up until a jump due to inner core nucleation. In our valid models, the onset of SiO_2 precipitation usually occurs in the first 1 Bya of Earth evolution (Fig. 4c), while the onset of MgO precipitation can occur up to more than 2 Bya after formation (Fig. 4d). Precipitation dominates the entropy production for the majority of these histories before inner-core nucleation (Fig. 4b), and both MgO and SiO_2 begin to precipitate prior to inner-core nucleation in all valid histories. Energy release from inner-core growth greatly increases the available entropy (Fig. 4a), decreases the core cooling rate (Fig. 4b) and suppresses precipitation of light elements (Fig. 4c-d). We find that the entropy contribution from the cooling term is, unsurprisingly, larger for higher initial CMB temperatures and is restricted to a small overall range for all valid model runs. In contrast, the available entropy from SiO_2 and MgO precipitation span a large range with a weak anti-correlation between the two terms.

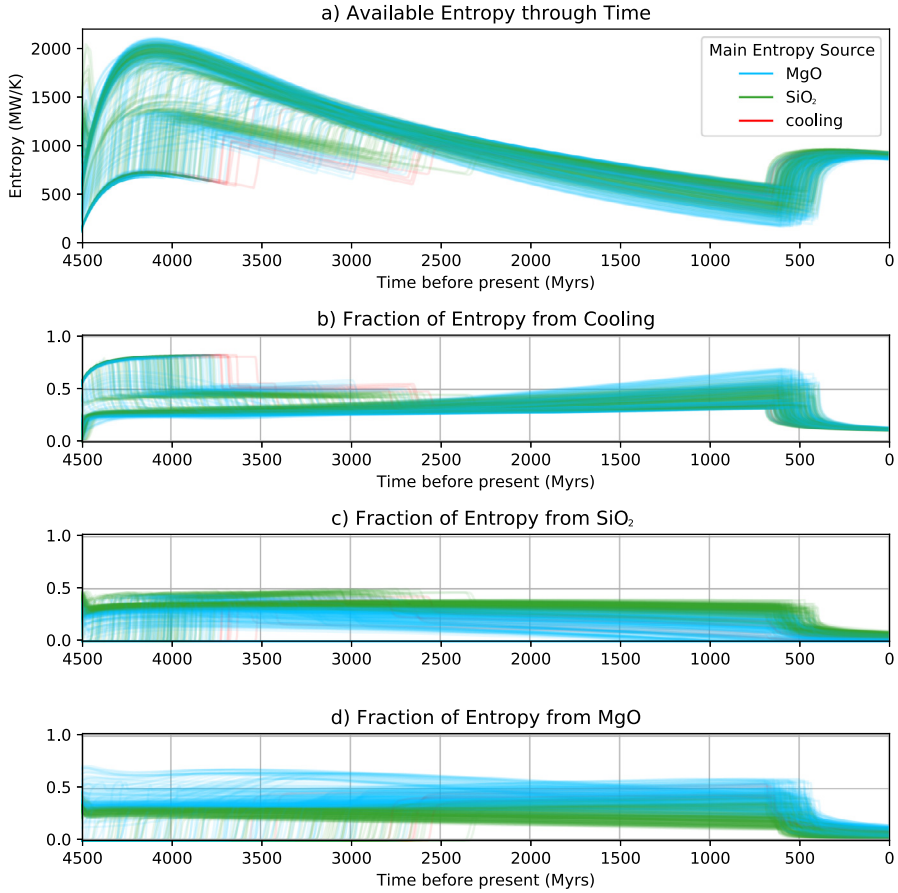

Fig. 4. Entropy production through time with Parameter Set 1 equilibrium coefficients (see Section 2.2, Badro et al. (2016); Fischer et al. (2015)). a) All permissible total available entropy histories through time with the color representing the time-averaged dominant entropy source (red=cooling, green=SiO_2, blue=MgO). The fractional contribution to the total available entropy over time by cooling (b), SiO_2 (c), and MgO (d) precipitation are shown in panels b-d. Cooling produces a significant fraction of total entropy, even in histories dominated by precipitation (b). In all histories, inner-core nucleation produces an increase in available entropy, and significantly decreases the entropy production of all other sources by decreasing the core cooling and precipitation rate.

For Parameter Set 2 (Fig. 5a), we find a similar trend in available entropy over time as for Parameter Set 1, but typically with much higher rates of precipitation and consequent entropy production. In contrast to the results in Fig. 4, the dominant entropy source is either precipitation of SiO_2 or FeO along with a few cases where MgO dominates. The light element precipitation always produces greater total available entropy through time than cooling though cooling still provides a substantial contribution to the available entropy (Fig. 5b). The sudden increases in available entropy due to the start of a light element precipitation reaction is limited to 4.5 and 3 Bya. Analogous to the other parameter set, the onset of SiO_2 precipitation usually occurs in the first 1.5 Bya of Earth evolution (Fig. 5c) whereas FeO precipitation generally starts almost always at the start in the early 10s of Mya of the model start time (Fig. 5e). After 3 Bya, the entropy histories are generally smooth until a jump due to inner core nucleation, though is more variance in the entropy histories between the SiO_2 and FeO dominated cases compared to Parameter Set 1. Akin to results from Parameter Set 1, the entropy contribution from the cooling term is restricted to a small overall range for all valid model runs while available entropy from SiO_2, FeO, and MgO precipitation spans a broad range with very weak anti-correlation between the three terms.

Although the results from Parameter Set 1 and Parameter Set 2 are to first-order similar in that all valid models have sufficient entropy available, the light elements that precipitate can be different. For instance, FeO precipitation can dominate entropy production for Parameter Set 2, whereas it is generally negligible for Parameter Set 1. The primary reason for this difference is that especially for FeO, the Parameter Set 2 distribution coefficients have a much stronger temperature as well as an overall lower equilibrium coefficient w.r.t. Parameter Set 1. This difference, in turn, leads to earlier and more rapid precipitation of oxygen and iron from the core. Additionally, this difference in equilibrium coefficients leads to most valid model histories with Parameter Set 2 having a much earlier onset of precipitation vis-a-vis Parameter Set 1.

This result illustrates that the choice of the equilibrium coefficients strongly affects model results and likely dominates over other sources of uncertainties.

5. Results & discussion: inner core nucleation

We find a consistent increase in available entropy at the onset of inner core nucleation (ICN) across all valid runs, in contrast with some previous work (Du et al., 2017) (Fig. 6). In general, we find a decrease in available entropy in 1 Byas before inner core nucleation (especially for Parameter Set 1), potentially suggesting a low magnetic field intensity before inner core nucleation. The timing of inner-core nucleation is not significantly affected by the strength of light-element precipitation using values from either Parameter Set 1 or Set 2, with both constants giving an inner-core age of 400-700 Mya (Fig. 6). Interestingly, these results are very consistent with recent measurements of low magnetic field intensity in the Ediacaran, which have been interpreted as a pre-cursory signature of inner core nucleation (Bono et al., 2019). However, we would note that the many uncertain parameters in both the core and mantle thermal model (e.g., mantle adiabat and melting

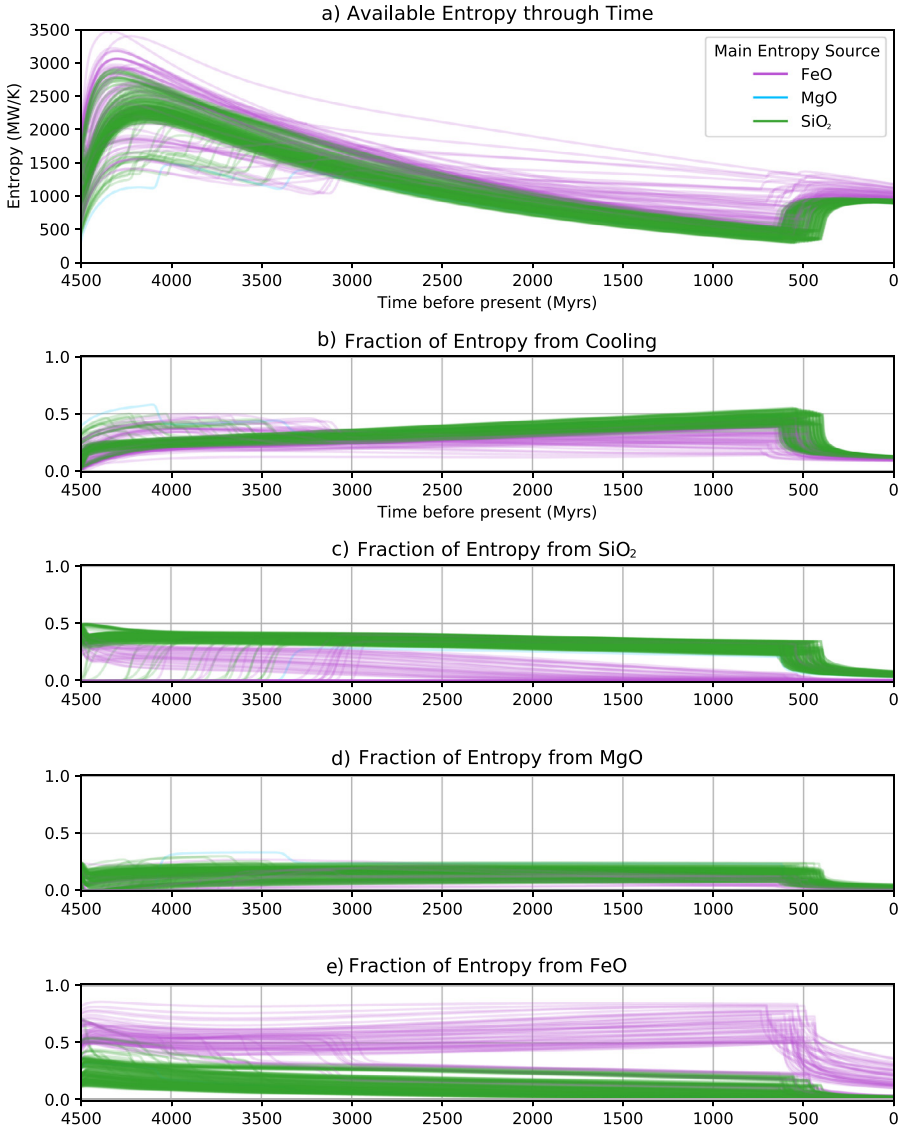

Fig. 5. Entropy production through time with Parameter Set 2 equilibrium coefficients (see Section 2.2, Badro et al. (2016); Hirose et al. (2017)). a) All permissible total available entropy histories through time with the color representing the time-averaged dominant entropy source (pink=FeO, green=SiO_2, blue=MgO). The precipitation always produces greater total available entropy through time than cooling. The fractional contribution to the total available entropy over time by cooling (b), SiO_2 (c), MgO(d), and FeO (e) precipitation are shown in panels b-e. Cooling produces a significant fraction of total entropy, even in histories dominated by precipitation (b). In all histories, inner-core nucleation produces an increase in available entropy, and significantly decreases the entropy production of all other sources by decreasing the core cooling and precipitation rate.

properties, mantle viscosity, and radiogenic heat production) can strongly impact the age of ICN (Davies, 2015; Nimmo, 2015) and hence our results should not be considered definitive.

However, the relationship between the strength of precipitation and the size of entropy increase with inner core nucleation, as well as the magnitude of entropy increase at ICN, is not the same for the two-parameter sets. We find that for Parameter Set 1, the entropy increase at ICN ranges from 50-350% and shows no clear relationship with either the average entropy from light element precipitation or what species is the dominant contributor to the available entropy (Fig. 6a, b). In contrast, the entropy increase at ICN ranges from 5-200% for Parameter Set 2, and there is a clear negative relationship between the strength of FeO precipitation and the size of the inner-core entropy jump (Fig. 6c, d).

It is important to note that ICN is commonly not the only entropy jump in our models. As illustrated in some of the model results in Fig. 3, Fig. 4, and Fig. 5, we find sudden increases in available entropy as different species begin to precipitate. Typically, these jumps occur before 2.5 Bya and should be distinguishable from an ICN jump. If these jumps produce observable signals in paleointensity records as has been suggested for ICN (e.g. Biggin et al., 2015; Smirnov et al., 2016; Sprain et al., 2018; Bono et al., 2019), the timing, and magnitude could provide constraints on the thermochemical evolution of Earth's core. We would, however, note that the relationship between core entropy production and field strength has uncertainties (e.g. Nimmo, 2015) that will have to be addressed to utilize the paleomagnetic observations.

6. Results & discussion: core compositional evolution

Our subset of valid model results allows us to directly track the evolution of the core composition over the Earth's history and compare it with constraints on the initial and present-day composition. All histories falling within the present-day seismic constraints and including more than 2 wt% O, as well as all histories falling within estimates for initial core compositions are plotted in Fig. 7a-b and Fig. 8a-b for Parameter Sets 1 and 2 respectively. The panel a for each of the figures shows the initial wt % of Si and O

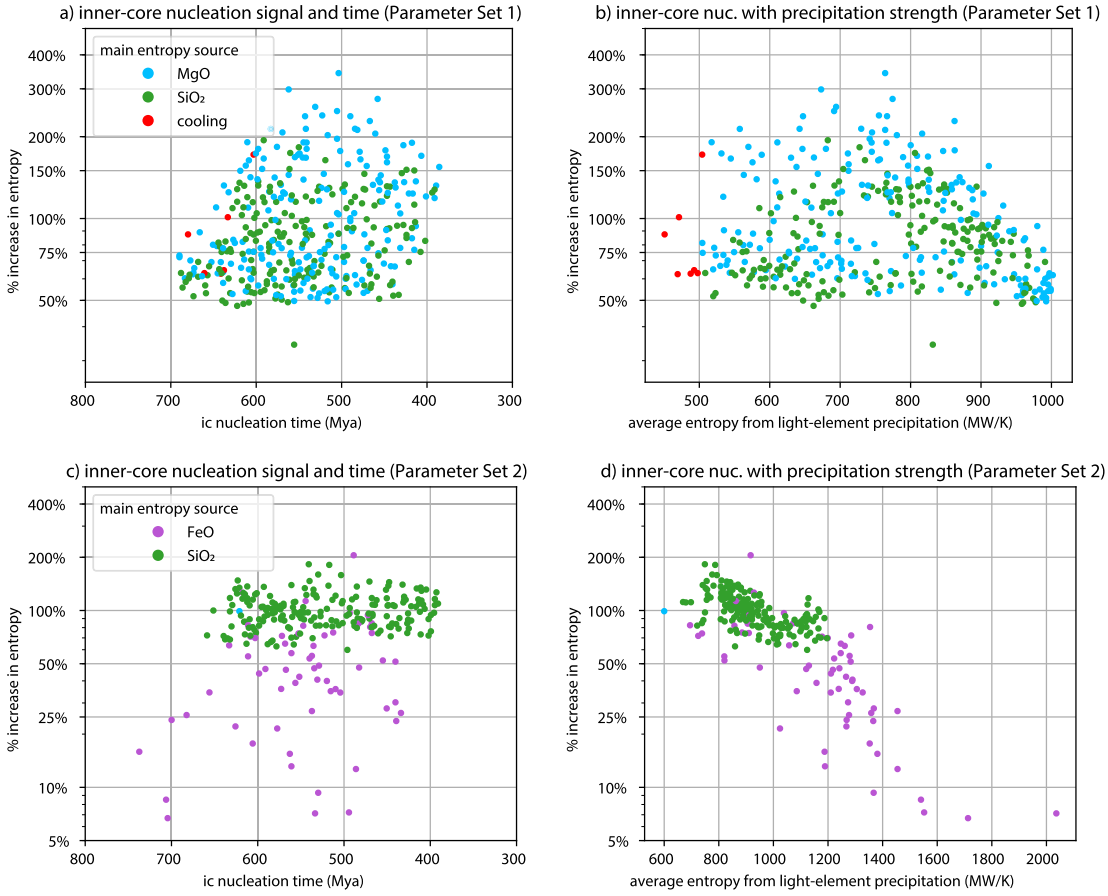

Fig. 6. Variations in the entropy increase from inner core nucleation depending on its nucleation timing (a, c) and precipitation strength (b, d) given Parameter Set 1 values Badro et al. (2016); Fischer et al. (2015) (a, b) and Parameter Set 2 values Badro et al. (2016); Hirose et al. (2017).

in the core for the allowed model runs whereas the panel b plots the present-day wt % of Si and O in the core fluid.

In our thermochemical models (within the parameter space we explored), it is difficult to evolve from an initial core with more silicon than oxygen as proposed by formation models to a present-day core with the opposite ratio as preferred by seismic constraints using either set of constants. We find that models run for Parameter Set 1 consistent with more reduced initial composition do not result in present-day cores that match seismic constraints when considering only Si, O, and Mg (Fig. 7b). Even allowing the inclusion of up to 3 wt% S and 7 wt% C (using seismic constraints from Badro et al. (2015)) only gives a few histories (Fig. 7b, yellow box) that satisfy both initial and final constraints at the very edge of each range. Besides, it is still unclear whether these few cases can explain the inner-core boundary density jump with less than 2 wt% oxygen (Alfè et al., 2002). This challenge of matching both constraints from formation models and seismic observations is even more significant with Parameter Set 2 (Fig. 8b).

On the other hand, estimates from formation models that satisfy seismic constraints for present-day compositions require oxidized initial conditions for the core for both Parameter Set 1 and Set 2. We find that all of the evolutionary histories consistent with present-day seismic constraints for Parameter Set 2 have negligible Si in the present-day core, and the dominant entropy source is FeO. In contrast, the present-day core can have up to 3 wt% Si for Parameter Set 2. Also, there is a strong trade-off between the permissible present-day core concentrations of Mg and O (Fig. S2 and S3) with cores that have more than 2 wt% oxygen also having less than 0.25 wt% Mg for both Parameter Sets. Likewise, there are trade-offs for the permissible range of present-day core Mg, Si, and O wt% s (Fig. S2 and S3). These model results are on account of two moles of oxygen precipitating with every mole of silicon. On average, histories using equilibrium constants for Parameter Set 1 lose between 0-1 wt% Si, 0.5-2 wt% O, and 0-2 wt% Mg over Earth's history (Fig. 7c-e) while the decrease is between 0-1.5 wt% Si, 0.5-6 wt% O, and 0-1 wt% Mg for Parameter Set 2 (Fig. 8c-e). Consequently, our results illustrate that the core can be significantly depleted in light elements at the present day compared to core formation. Liu et al. (2019) find broadly similar results with their analysis and require a Si and O-rich initial core composition to produce light element precipitation for all of Earth's history.

We would note that our results do not definitively show that estimates of initial core composition and modern composition are in conflict with each other given the large potential parameter space and model simplifications (see Supplement Section S2.2, S2.4, S4; see discussion in Section S7.1). However, our results do illustrate that light precipitation from the core and its coupling with mantle processes is an important process for the core compositional evolution and should be explicitly considered in future models.

7. Conclusions

We have used a coupled chemical thermodynamic framework to calculate the energy budget and chemical interaction over the entire history of the Earth's core. We find that for a wide range of parameter space, precipitation of three light element species – MgO, SiO_2, and FeO – can provide sufficient entropy to drive the dynamo with multiple species precipitating in most cases (see more discussion in Supplementary S7).

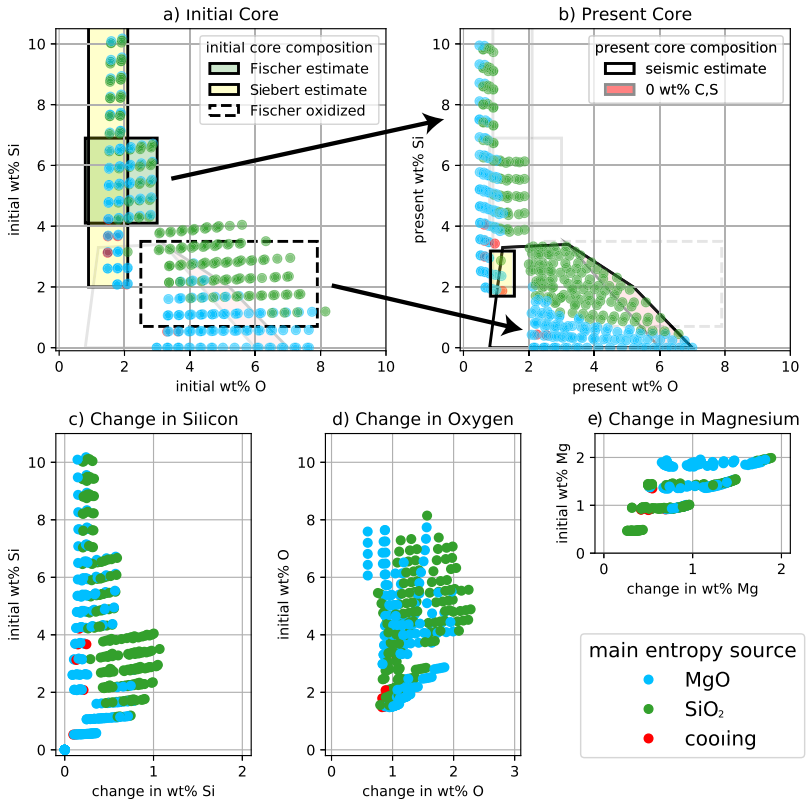

Fig. 7. Parameter Set 1: Viable model runs matching either a) the initial core composition, (b) the present day core composition, or both, and the corresponding change in (c) silicon content, (d) oxygen content, and (e) magnesium content for these models. The arrows in the figure illustrate the mapping between initial and present-day core compositions.

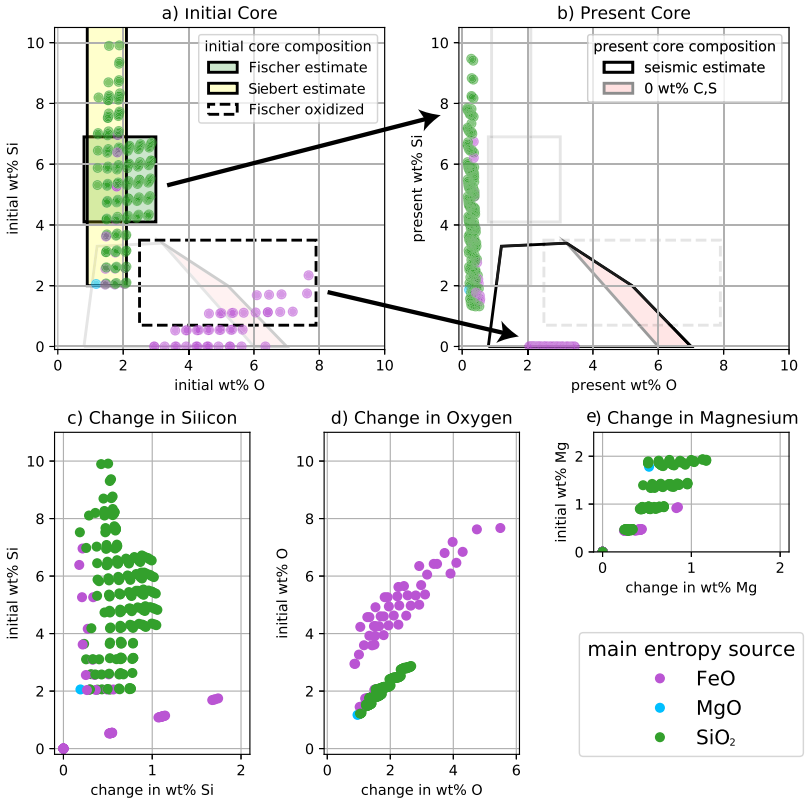

Fig. 8. Parameter Set 2: Viable model runs matching either a) the initial core composition, (b) the present day core composition, or both, and the corresponding change in (c) silicon content, (d) oxygen content, and (e) magnesium content for these models. The arrows in the figure illustrate the mapping between initial and present-day core compositions.

In previous studies, the mantle side of the precipitation reaction was not adequately taken into consideration. We find that the precipitated MgO, SiO_2, and FeO that collects in the interaction layer buffers further precipitation until the layer is swept away by background mantle convection. This process alters the timescale of precipitation and hence, entropy production available to power Earth's early dynamo. The "conveyor belt" mechanism resulting from mantle convection prevents the interaction layer containing precipitated chemical species MgO, FeO, and SiO_2 from growing large enough to become buoyantly unstable in contrast with what has been previously suggested (Helffrich et al., 2017) making it difficult to detect through seismic or geochemical signatures (see Supplementary Section 6 for more discussion). Nevertheless, our results highlight the potential importance of light precipitation for the core compositional evolution as well as the possibility of different light elements being precipitated at different times in Earth's history. We expect that with improved experimental and ab-initio results as well as a broad parameter space exploration, a modeling framework as outlined in this study can better help constrain the compositional evolution of the Earth's core and its thermal history over its full lifetime.

Author contributions

All the authors on the paper were involved in developing the project with T.M. and N.K. taking the lead in developing the model, writing the Python code, and analyzing the results. T.M. and N.K. were primarily responsible for writing the manuscript along with substantial contribution by C.W., C.M., and S.A. J.L. significantly helped with the framing of the work (especially the nature of chemical exchange and formulating the thermodynamic model) and provided a lot of guidance throughout the project and the manuscript while T.J. performed numerical simulations to help develop the idea of the mantle conveyor belt. Correspondence and requests for materials should be addressed to Tushar Mittal (email: tmittal2@berkeley.edu). The code for the analysis in the paper is available at https://doi.org/10.6084/m9.figshare.9588854.v4.

Declaration of competing interest

We do not have any conflict of interest with regards to this study.

Acknowledgements

We would like to thank the CIDER summer program (EAR #1135452) for the possibility to participate in the 2016 summer workshop where this project started. We would also like to thank Bruce Buffet, Raymond Jeanloz, Brent Delbridge, Anat Shahar, Razvan Caracas, Rich Walker, and Michael Manga for useful discussions that helped develop this study. We also would like to thank the Editor John Brodholt and the reviewer for careful suggestions which significantly helped improve the clarity and focus of the manuscript. The authors declare that they have no competing financial interests. The scripts for the model presented in the paper are available as supplementary file. We acknowledge graduate funding support for T.M. from the NSF grant EAR #1615203, NSF Postdoctoral Program EAR-PF-1349811 for C.W., NSF grant EAR #1522560 for C.M., NASA grant NNX15AG54G for J.L.

Appendix A. Supplementary material

Supplementary material related to this article can be found online at https://doi.org/10.1016/j.epsl.2019.116030.

References

Alfè, D., Gillan, M., Price, G.D., 2002. Composition and temperature of the Earth's core constrained by combining ab initio calculations and seismic data. Earth Planet. Sci. Lett. 195, 91–98.

Alfè, D., Price, G., Gillan, M., 2004. The melting curve of iron from quantum mechanics calculations. J. Phys. Chem. Solids 65, 1573–1580. https://doi.org/10.1016/j.jpcs.2003.12.014. http://linkinghub.elsevier.com/retrieve/pii/S0022369704000538.

Badro, J., Aubert, J., Hirose, K., Nomura, R., Blanchard, I., Borensztajn, S., Siebert, J., 2018. Magnesium partitioning between Earth's mantle and core and its potential to drive an early exsolution geodynamo. Geophys. Res. Lett. 45, 13–240.

Badro, J., Brodholt, J.P., Piet, H., Siebert, J., Ryerson, F.J., 2015. Core formation and core composition from coupled geochemical and geophysical constraints. Proc. Natl. Acad. Sci. 112, 12310–12314.

Badro, J., Siebert, J., Nimmo, F., 2016. An early geodynamo driven by exsolution of mantle components from Earth's core. Nature 536, 1–3. https://doi.org/10.1038/nature18594. https://doi.org/10.1017/CBO9781107415324.004.

Biggin, A., Piispa, E., Pesonen, L., Holme, R., Paterson, G., Veikkolainen, T., Tauxe, L., 2015. Palaeomagnetic field intensity variations suggest mesoproterozoic inner-core nucleation. Nature 526, 245.

Bono, R.K., Tarduno, J.A., Nimmo, F., Cottrell, R.D., 2019. Young inner core inferred from ediacaran ultra-low geomagnetic field intensity. Nat. Geosci. 12, 143.

Chidester, B.A., Rahman, Z., Righter, K., Campbell, A.J., 2017. Metal–silicate partitioning of u: implications for the heat budget of the core and evidence for reduced u in the mantle. Geochim. Cosmochim. Acta 199, 1–12.

Davies, C.J., 2015. Cooling history of Earth's core with high thermal conductivity. Phys. Earth Planet. Inter. 247, 65–79.

Driscoll, P., Bercovici, D., 2014. On the thermal and magnetic histories of Earth and Venus: influences of melting, radioactivity, and conductivity. Phys. Earth Planet. Inter. 236, 36–51.

Du, Z., Jackson, C., Bennett, N., Driscoll, P., Deng, J., Lee, K.K., Greenberg, E., Prakapenka, V.B., Fei, Y., 2017. Insufficient energy from mgo exsolution to power early geodynamo. Geophys. Res. Lett. 44.

Fischer, R.A., Campbell, A.J., Ciesla, F.J., 2017. Sensitivities of Earth's core and mantle compositions to accretion and differentiation processes. Earth Planet. Sci. Lett. 458, 252–262.

Fischer, R.A., Nakajima, Y., Campbell, A.J., Frost, D.J., Harries, D., Langenhorst, F., Miyajima, N., Pollok, K., Rubie, D.C., 2015. High pressure metal–silicate partitioning of Ni, Co, V, Cr, Si, and O. Geochim. Cosmochim. Acta 167, 177–194.

Foley, B.J., Bercovici, D., 2014. Scaling laws for convection with temperature-dependent viscosity and grain-damage. Geophys. J. Int. 199, 580–603.

Gomi, H., Ohta, K., Hirose, K., Labrosse, S., Caracas, R., Verstraete, M.J., Hernlund, J.W., 2013. The high conductivity of iron and thermal evolution of the Earth's core. Phys. Earth Planet. Inter. 224, 88–103.

Helffrich, G., Ballmer, M., Hirose, K., 2017. Core-exsolved SiO_2 dispersal in the Earth's mantle. J. Geophys. Res., Solid Earth, 176–188. https://doi.org/10.1002/2017JB014865.

Hirose, K., Labrosse, S., Hernlund, J., 2013. Composition and state of the core. Annu. Rev. Earth Planet. Sci. 41, 657–691.

Hirose, K., Morard, G., Sinmyo, R., Umemoto, K., Hernlund, J., Helffrich, G., Labrosse, S., 2017. Crystallization of silicon dioxide and compositional evolution of the Earth's core. Nature 543, 99–102. https://doi.org/10.1038/nature21367.

Keller, B., Schoene, B., 2018. Plate tectonics and continental basaltic geochemistry throughout Earth history. Earth Planet. Sci. Lett. 481, 290–304.

de Koker, N., Steinle-Neumann, G., Vlček, V., 2012. Electrical resistivity and thermal conductivity of liquid Fe alloys at high P and T, and heat flux in Earth's core. Proc. Natl. Acad. Sci. 109, 4070–4073.

Konopkova, Z., McWilliams, R.S., Gómez-Pérez, N., Goncharov, A.F., 2016. Direct measurement of thermal conductivity in solid iron at planetary core conditions. Nature 534, 99–101. https://doi.org/10.1038/nature18009.

Labrosse, S., 2015. Thermal evolution of the core with a high thermal conductivity. Phys. Earth Planet. Inter. 247, 36–55. https://doi.org/10.1016/j.pepi.2015.02.002. http://linkinghub.elsevier.com/retrieve/pii/S0031920115000175.

Liu, W., Zhang, Y., Yin, Q.Z., Zhao, Y., Zhang, Z., 2019. Magnesium partitioning between silicate melt and liquid iron using first-principles molecular dynamics: implications for the early thermal history of the Earth's core. Earth Planet. Sci. Lett., 115934.

Müller, R.D., Seton, M., Zahirovic, S., Williams, S.E., Matthews, K.J., Wright, N.M., Shephard, G.E., Maloney, K.T., Barnett-Moore, N., Hosseinpour, M., et al., 2016. Ocean basin evolution and global-scale plate reorganization events since Pangea breakup. Annu. Rev. Earth Planet. Sci. 44, 107–138.

Nimmo, F., 2015. Energetics of the Core. Elsevier B.V.

Ohta, K., Kuwayama, Y., Hirose, K., Shimizu, K., Ohishi, Y., 2016. Experimental determination of the electrical resistivity of iron at Earth's core conditions. Nature 534, 95–98. https://doi.org/10.1038/nature17957.

Oka, K., Hirose, K., Tagawa, S., Kidokoro, Y., Nakajima, Y., Kuwayama, Y., Morard, G., Coudurier, N., Fiquet, G., 2019. Melting in the Fe-FeO system to 204 GPa: implications for oxygen in Earth's core. Am. Mineral. 104, 1603–1607.

Olson, P., 2013. The new core paradox. Science 342, 431–432.

O'Rourke, J.G., Stevenson, D.J., 2016. Powering Earth's dynamo with magnesium precipitation from the core. Nature 529, 387–389. https://doi.org/10.1038/nature16495. http://www.nature.com/doifinder/10.1038/nature16495.

Piet, H., Badro, J., Gillet, P., 2017. Geochemical constraints on the size of the moon-forming giant impact. Geophys. Res. Lett. 44, 11–770.

Piper, J.D., 2013. A planetary perspective on Earth evolution: lid tectonics before plate tectonics. Tectonophysics 589, 44–56.

Poirier, J.P., 1994. Light elements in the Earth's outer core: a critical review. Phys. Earth Planet. Inter. 85, 319–337.

Pozzo, M., Davies, C., Gubbins, D., Alfè, D., 2013. Transport properties for liquid silicon-oxygen-iron mixtures at Earth's core conditions. Phys. Rev. E 87, 014110.

Pozzo, M., Davies, C., Gubbins, D., Alfè, D., 2012. Thermal and electrical conductivity of iron at Earth's core conditions. Nature 485, 355–358. https://doi.org/10.1038/nature11031. http://adsabs.harvard.edu/cgi-bin/nph-data_query?bibcode=2012Natur.485..355P%26link_type=ABSTRACT.

Rubie, D.C., Jacobson, S.A., Morbidelli, A., O'Brien, D.P., Young, E.D., de Vries, J., Nimmo, F., Palme, H., Frost, D.J., 2015. Accretion and differentiation of the terrestrial planets with implications for the compositions of early-formed solar system bodies and accretion of water. Icarus 248, 89–108.

Siebert, J., Badro, J., Antonangeli, D., Ryerson, F.J., 2012. Metal–silicate partitioning of Ni and Co in a deep magma ocean. Earth Planet. Sci. Lett. 321, 189–197.

Siebert, J., Badro, J., Antonangeli, D., Ryerson, F.J., 2013. Terrestrial accretion under oxidizing conditions. Science 339, 1194–1197.

Smirnov, A.V., Tarduno, J.A., Kulakov, E.V., McEnroe, S.A., Bono, R.K., 2016. Palaeointensity, core thermal conductivity and the unknown age of the inner core. Geophys. J. Int. 205, 1190–1195.

Sprain, C.J., Swanson-Hysell, N.L., Fairchild, L.M., Gaastra, K., 2018. A field like today's? The strength of the geomagnetic field 1.1 billion years ago. Geophys. J. Int. 213, 1969–1983.

Stevenson, D.J., Spohn, T., Schubert, G., 1983. Magnetism and thermal evolution of the terrestrial planets. Icarus 54, 466–489. https://doi.org/10.1016/0019-1035(83)90241-5. http://adsabs.harvard.edu/cgi-bin/nph-data_query-bibcode=1983Icar...54..466S%26link_type=ABSTRACT.

Tarduno, J.A., Cottrell, R.D., Davis, W.J., Nimmo, F., Bono, R.K., 2015. A Hadean to Paleoarchean geodynamo recorded by single zircon crystals. Science. http://www.sciencemag.org/content/349/6247/521.short.

Weller, M.B., Lenardic, A., 2018. On the evolution of terrestrial planets: bi-stability, stochastic effects, and the non-uniqueness of tectonic states. Geosci. Front. 9, 91–102.

Williams, Q., 2018. The thermal conductivity of Earth's core: a key geophysical parameter's constraints and uncertainties. Annu. Rev. Earth Planet. Sci. 46, 47–66.

Yong, W., Secco, R.A., Littleton, J.A., Silber, R.E., 2019. The iron invariance: implications for thermal convection in Earth's core. Geophys. Res. Lett.